Theoretical studies on alloying of germanene supported on Al (111) substrate*

Qian-Xing Chen(陈前行)[1], Hao Yang(杨浩)[1], and Gang Chen(陈刚)[1,2,†]

[1] *Laboratory of Advanced Materials Physics and Nanodevices, School of Physics and Technology, University of Jinan, Jinan* 250022, *China*
[2] *School of Physics and Electronics, Shandong Normal University, Jinan* 250358, *China*

(Received 4 April 2020; revised manuscript received 30 May 2020; accepted manuscript online 12 June 2020)

Using density functional theory, we study the alloying of the buckled hexagonal germanene superlattice supported on Al (111)-(3 × 3), the sheet composed of triangular, rhombic, and pentagonal motifs on Al (111)-(3 × 3), and the buckled geometry on Al (111)-($\sqrt{7}\times\sqrt{7}$)(19°), which are denoted, respectively, by BHS, TRP, and SRT7, to facilitate the discussion in this paper. They could be alloyed in the low doping concentration range. The stable configurations BHS, TRP, and SRT7 of the pure and alloyed germanenes supported on both Al (111) and its Al_2Ge surface alloy, except the SRT7 pure germanene on Al_2Ge, could re-produce the experimental scanning tunneling microscopy images. The relatively stable Al–Ge alloy species are the Al_3Ge_5 BHS-2T, Al_3Ge_5 TRP-2T, and Al_3Ge_3 SRT7-1T on Al (111) while they are the Al_4Ge_4 BHS-1T, Al_3Ge_5 TRP-2T, and $Al_{27}Ge_{27}$ SRT7-(3×3)-9T on Al_2Ge (the *n* in the *n*T means that there are *n* Ge atoms per unit which sit at the top sites and protrude upward). In addition, the Al_3Ge_5 BHS-2T and Al_4Ge_4 BHS-1T are the most stable alloy sheets on Al (111) and Al_2Ge, respectively. Comparing with the experimental studies, there exists no structural transition among these alloyed configurations, which suggests that the experimental conditions play a crucial role in selectively growing the pure or the alloyed germanene sheets, which may also help grow the one-atomic thick honeycomb structure on idea Al (111).

Keywords: first-principles calculation, alloyed two-dimensional material, substrate for two-dimensional material growth, two-dimensional nanostructure

PACS: 81.05.Zx, 81.05.Rm, 81.05.ue, 81.07.–b **DOI:** 10.1088/1674-1056/ab9c08

1. Introduction

Since the invention of the single layer graphene, the two-dimensional (2D) materials have gained extraordinarily intensive research attention due to their peculiar properties for both fundamental studies and application investigations.[1–5] Most of the two-dimensional (2D) structures could be isolated from their corresponding layered bulk materials, such as the graphene,[1,2,6] 2D transition metal carbides and carbonitrides,[7] transition metal dichalcogenides,[8–10] and black phosphorus.[11] Germanene, the same column counterpart of graphene, is another 2D material which has no layered crystal material in nature and can only be grown in experiment.[12–24] The closely packed (111)-oriented metallic surfaces are usually used as substrates to support the 2D material syntheses. In addition, the supported 2D nanostructures rather than the free-standing ones would probably be required for most cases of applications. However, the currently used substrates are usually the precious noble metals, such as the Pt, Au, and Ag, which are so expensive that their usage is limited. Therefore, the search for cheap substances for supporting 2D materials is urgent.

Interestingly, the germanene has been successfully synthesized on an Al (111) surface.[14–20] As the result of the sp^2–sp^3 hybridization mixing, the free-standing germanene has the slightly buckled structure as a ground state, which would change to show different structural characteristics on supporting substrates, which is attributed to the interface interaction, such as the germanene superlattice to topologically match the Pt (111)-$\left(\sqrt{19}\times\sqrt{19}\right)$ (23.4°) unit synthesized by Li *et al.*,[12] the germanene superlattice grown on Au (111)-$\left(\sqrt{7}\times\sqrt{7}\right)$ (19.1°) by Dávila *et al.*[13] Recently, several structural models containing 8 Ge atoms in a corresponding unit cell to topologically match the Al (111)-(3 × 3) periodicity were proposed.[14–17] In 2015, Derivaz *et al*. reported the first experimental study of germanene on Al (111), in which the buckled hexagonal superlattice with two Ge atoms adsorbed on top of the Al atoms being protruded upward in the unit cell (BHS-2T model) was used to explain their scanning tunneling microscopy (STM) image.[14] In the total-reflection high-energy positron diffraction study, Fukaya *et al*. found only one protrudued Ge atom in the unit cell and proposed the BHS-1T model.[15] In 2017, the buckled hexagonal superlattice with a Ge atom adsorbed at the 3-fold hollow site protruded upward in the unit (BHS-1H model) was independently found by Stephan *et al.*[16] and Wang and Uhrberg.[17] Interestingly, Stephan *et al*. found experimentally that the BHS-2T and BHS-1H models could transit to each other quite easily.[16] Besides, the germanane superlattice with one pro-

*Project supported by the National Natural Science Foundation of China (Grant No. 11674129).
†Corresponding author. E-mail: phdgchen@163.com

truded Ge atom in the 6-atom unit grown on an Al (111)-$\left(\sqrt{7}\times\sqrt{7}\right)$ (19.1°) reconstructed surface was also proposed in experiment.[17,18] Surprisingly, Martínez *et al*. found that only Al–Ge alloy sheets were grown on Al (111) instead of the pure germanene in their experimental studies, and proposed an structural model composed of triangular, rhombic, and pentagonal structural motifs (TRP model).[20] Thus, the questions whether the previous models are correct or not and whether the well-controlled experimental conditions could be used to selectively synthesize pure or alloyed germanene sheets on purpose are naturally raised.

In this paper, we carefully study the alloying of the buckled germanene configurations which were previously reported for the experimentally fabricated germanene sheets supported on Al (111) substrate. Providing there are available Al atoms to take part in the germanene fabrication reaction, the buckled germanene configurations could be alloyed in the range of the low doping concentration. The Al atoms may come from the vacancy defect in Al (111), the Al atoms on the edge of the surface step, the introduced Al atoms as guest atom along with the Ge atom source, or the ones taken out from the top surface of Al (111) by the kinetic energy of the incoming Ge atoms or the energy released during the formation of germanene-based sheet. In Section 2, we provide the computational details of our studies. The calculated results on the alloying of the germanene sheets supported on the pristine Al (111) surface are presented in Subsection 3.1. With the purpose to benefit further experimental investigation of large-quantity fabrication of germanene, we also evaluate the effects of the interface interaction modification on the alloying of germanene in Subsection 3.2. And, to give a comprehensive understanding of the structural candidates of the experimental observed alloy sheets and the possibility of isolating the fabricated sheets the results are discussed in Subsection 3.3. Some conclusions are drwan from of this study in Section 4. Our detailed studies on the alloying of the germanene configurations could on one hand answer the question whether the pure or the alloyed structures growon Al (111) surface and on the other hand help design novel 2D nanostructures for high-performance nanodevices.

2. Computational details

The spin-polarized density functional theory calculations were carried out by using the Vienna ab initio simulation package.[25] The generalized gradient approximation with the Perdew, Bure, and Ernzerhof (PBE) functional was used to calculate the exchange and correlation energy.[26] The projector augmented wave (PAW) potential was adopted to account for the ion–electron interaction.[27] The plane wave basis with the cutoff energy of 312.3 eV was used to construct the wavefunction. In order to simulate the Al (111) surface, we used a 6-layer slab with the two bottom layers frozen to mimic the bulk effects, which is separated by 14-Å vacuum space to eliminate the effects from its periodic images. All the other atoms in the slab were fully relaxed until the calculated Hellmann–Feynman forces meet the convergence tolerance of 5 meV/Å. The electronic properties converged to 10^{-5} eV. In our study, the substrates as the Al (111)-$\left(\sqrt{7}\times\sqrt{7}\right)$ (19.1°), Al (111)-(3×3), Al (111)-$\left(\sqrt{19}\times\sqrt{19}\right)$ (23.4°), and Al (111)-(6×6) were used to topologically match the supported 2D structural models, whose first Brillouin zones were sampled by using the $9\times9\times1$, $7\times7\times1$, $5\times5\times1$, and $3\times3\times1$ Monkhorst–Pack k-meshes,[28] respectively. In order to have examine the accuracy of our calculation method, we calculate the lattice constants of the fcc Al bulk and the diamond Ge bulk, which are calculated to be 4.04 Å and 5.78 Å, these values being in agreement with the experimental values of 4.05 Å and 5.66 Å.[29]

The free-standing germanene has the low-buckled structure as ground state consisting of two sublattices with one of them being vertically displaced with respect to the other one. In our study, the in-plane lattices of the low-buckled germanene are calculated to be $\sim$ 4.06 Å and the displacement height between the sublattices is found to be $\sim$ 0.69 Å, which are coincide with the previously reported data.[30,31] We also calculated the Al_2, Ge_2, and AlGe dimer. The bond lengths of the $^3\Sigma_g$ triplet ground states of Al_2 and Ge_2 dimers are found to be 2.488 Å and 2.426 Å, which are in agreement with the experimental data of 2.48 Å and 2.44 Å, respectively.[32,33] The $^4\Sigma$ quadruple state of AlGe dimer is calculated to have the 2.486 Å bond length, which is in accordance with the previously reported theoretical value of 2.491 Å.[34]

3. Results and discussion

3.1. The alloying of germanene on the pristine Al (111)

Using the previously proposed structural models of germanenes on the Al (111) surface, we carefully optimize the geometries and show their results in Fig. 1. In experiment, the bulked hexagonal superlattices BHS-2T and BHS-1H are used to explain the scanning tunneling microscopy images of the germanenes grown on Al (111)-(3×3),[14,16,17] which has two Ge atoms at the top sites and one Ge atom at the 3-fold hollow site protruded upward. However, these geometries are higher in energy than the honeycomb lattice (HL) and the Kagome lattice (KL) configurations found in the first-principles studies of the germanenes grown on Al (111).[35] Recently, a novel configuration TRP-1T was proposed for the Al–Ge alloy sheet supported on Al (111). For pure germanene, there are two Ge atoms adsorbed at the top sites in the unit cell of TRP-1T structure: one of them is in the center of the Ge_6 ring having 3 nearest Ge atoms (2.60 Å away) and 3 next nearest Ge (3.47 Å away), vertically displaced by 1.16 Å and referred

to as the basal plane of germanene, and the other T-site Ge atom at the vertex co-shared by three adjacent Ge_5 pentagons is only lifted by ~ 0.4 Å. As discussed later in this paper, only the Ge atom in the center of Ge_6 ring could be clearly seen in the simulated STM image. Besides, we also consider the structural models of the germanenes grown on the Pt (111)-$\left(\sqrt{19}\times\sqrt{19}\right)$ (23.4°) and the Al (111)-$\left(\sqrt{7}\times\sqrt{7}\right)$ (19.1°), which we would like to refer to as the SRT19 and SRT7 models respectively to facilitate the discussion of them. On Al (111), the SRT19 and SRT7 are found to have three Ge atoms and one Ge atom at top sites protruded upward in the corresponding unit cells, respectively. In fact, the protruded Ge atoms in the SRT19-3T model slightly deviate from the top sites. The height increases of the protruded Ge atoms are about 1.25, 1.62, 1.39, and 1.43 Å on average of the BHS-2T, BHS-1H, SRT19-3T, and SRT7-1T models, respectively. In view of the energetic stabilities, we calculate the energy release ($E_{\rm er}$) to estimate the cohesive energy of germanene itself and the adsorption energy of germanene on Al (111) from the following formula:

$$E_{\rm er} = \frac{NE_{\rm Ge} + E_{\rm substrate} - E_{\rm total}}{N}, \tag{1}$$

where the $E_{\rm Ge}$, $E_{\rm substrate}$, and $E_{\rm total}$ are the energy of a free-standing Ge atom, the substrate, and the germanene supported on the substrate, respectively. In line with previous studies, the HL is the energetically favorable configuration on Al (111), whose $E_{\rm er}$ is 47, 69, 78, 85, 69, and 66 meV/atom higher than that of the KL, TRP-1T, BHS-2T, BHS-1H, SRT19-3T, and SRT7-1T configurations, respectively. However, such a honeycomb geometry could not re-produce the bright spot pattern of the observed STM image.[14,16,17]

Inspired by the experimental study of the Al–Ge alloy sheet supported on Al (111), we examine whether the alloying of germanene with Al could account for the discrepancy between the theoretical results and the experimental observations. Starting from the above mentioned germanene models, we study the alloying process by substationally doping Al atoms one by one. First, we use the supercells with the in-plane lattices longer than 12.3 Å to investigate the doping configurations of a single Al atom in the germanene models (see Fig. A1 in Appendix A: Supporting information). Among the structural configurations, only BHS-1H model has the protruded Ge atoms at the 3-fold hollow site of the Al (111) substrate, for which the single Al doping prefers to replace the protruded Ge atom. Then, the doped Al would lower down to the basal plane of the germanene to directly develop three Al–Al bonds with the substrate, making its surrounding Ge atoms slightly lifted (~ 0.54 Å). In the SRT19-3T, SRT7-1T, BHS-2T, and TRP-1T models, the single Al atom favors the nearest multi-coordination site next to the protruded Ge atom to maximize its coordination number with the substrate. In the SRT19-3T model, the replacing of a protruded Ge atom, would cause one of its nearest Ge atoms to pop up, which has the energy about 35 meV higher than the original one. In all the other models, the replacing of the protruded Ge atoms with Al atoms results in its energy more than 0.3 eV higher than the total energy. Also, our calculations support the next-nearest neighboring doping of two Al atoms (see Fig. A2 in Appendix A: Supporting information). For SRT19, SRT7, BHS, and TRP models, the nearest doping of two Al atoms results in its energy 0.22 eV higher than total energy, thus ruling out the formation of Al_2 dimer. However, the formations of Al_2 dimers lead to only 0.01 eV and 0.07 eV higher in HL and KL models, respectively. This may be attributed to the fact that neither HL nor KL is unlike to be alloyed, which will be discussed later in this paper.

Due to the intensive computing loading of the calculations using supercells, we then adopt the smallest units of the corresponding models, except the supercell to match the Al (111)-(3×3) for HL model, and to study the alloying processes step by step. For each doping concentration, the configurations are carefully studied and the lowest energy configuration is selected as the corresponding alloy configuration. In the alloying process, the relative energy release $\left(\Delta E_{\rm er}^{\rm alloy}\right)$ referring to the energy release of the pure HL germanene $\left(E_{\rm er}^{\rm HL}\right)$, and the step wise formation energy ($E_{\rm swf}$) as defined below are studied:

$$\Delta E_{\rm er}^{\rm alloy} = \frac{ME_{\rm Al} + NE_{\rm Ge} + E_{\rm substrate} - E_N}{M+N} - E_{\rm er}^{\rm HL}, \tag{2}$$

$$E_{\rm swf} = E_{N-1} + \mu_{\rm Al} - E_N - \mu_{\rm Ge}, \tag{3}$$

where the $E_{\rm Al}$, E_{N-1}, and E_N are the energy of a free-standing Al atom and the energy per unit cell of the Al–Ge alloy sheet containing $N-1$ and N substitutionally doped Al atoms, respectively. The $E_{\rm er}^{\rm HL}$ is the energy calculated from formula (1) for HL pure germanene. The M represents the number of Ge atoms in the studied unit. The $\mu_{\rm Al}$ ($\mu_{\rm Ge}$) is the chemical potential calculated as the energy per Al (Ge) atom of the corresponding bulk. The positive $E_{\rm swf}$ refers to the exothermic reaction to favor the corresponding alloy formation. As to the HL and KL germanene model, the calculated $E_{\rm swf}$ is always negative to hinder their alloying with Al. The BHS-1H configuration could not remain. For the alloy configuration with only one Al atom in the unit cell of the BHS-1H model, the doped Al prefers to replace the protruded Ge and reduce the height to bond with the substrate. However, such a configuration would quickly transit to the corresponding single Al doped BHS-2T configuration under ~ 26 meV activation energy, which is exothermic to release of ~ 0.1 eV/unit energy. Furthermore, the two-Al-atoms-doped BHS-1H would change to the corresponding BHS-2T configuration immediately without energy barrier. So, we can say that there would be no BHS-1H structural model for the Al–Ge alloy sheet on the Al (111) substrate.

Another special model is the TRP-1T. For the TRP-1T model, the undoped germanene has only one Ge atom obviously protruded upward (see Fig. 1). The Ge atom at the vertex, which is jointly shared by three Ge_5 pentagons, is only slightly lifted, which would however pop upward in the alloyed configuration that can be seen in the STM study. For the SRT19 model, the three protruded Ge atoms in the unit cell would remain until the number of the doped Al atoms increases to 6. In the configuration with 7 Al atoms, one of the protruded Ge atoms would be lowered down to the basal germanene plane. In the Al alloyed SRT19 models with 8 and 9 Al atoms, there is only one Ge atom kept on the germanene basal plane in the corresponding unit cell. In our study, only the SRT7-1T and BHS-2T configuration are found to preserve their structural characteristics in the alloying process. In Fig. 2, one can see that the corresponding critical concentrations for $E_{\rm swf}$ transitions from positive to negative are Al:Ge = 9:9 for SRT19, 3:3 for SRT7, and 3:5 for TRP and BHS configurations, respectively. The alloy configurations with the positive $E_{\rm swf}$ are shown in Fig. 3 and the others with negative values are displayed in Fig. A3 in Appendix A: Supporting information. In the alloy configurations shown in Fig. 3, the Al atom favors the doping site next to the protruded Ge atom. Also, the neighboring doping site for Al atom is the next nearest one.

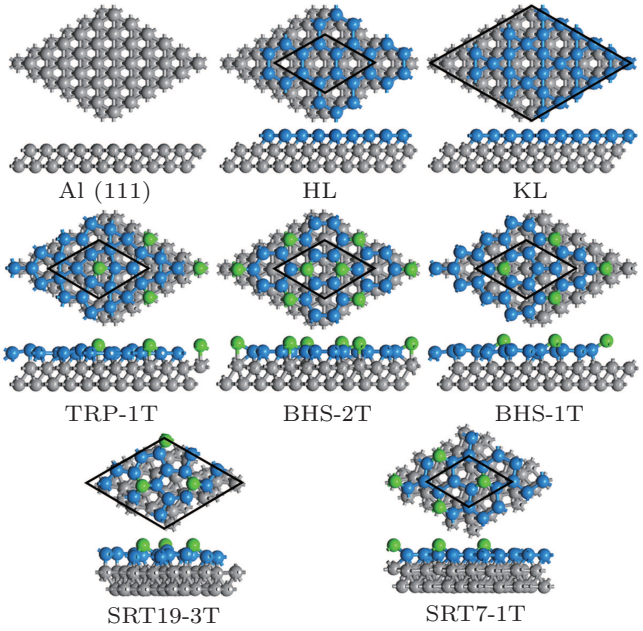

Fig. 1. Schematic illustrations of structural models of germanenes grown on Al (111) along with the configuration of the Al (111) itself. Only two top layers of substrate are shown. Black rhombuses are periodic units used in calculations. Grey, blue, and green spheres represent Al atoms in substrate, Ge atoms in basal plane of the 2D sheet, and Ge atoms protruded upward which can be seen in STM image of the 2D sheet, respectively.

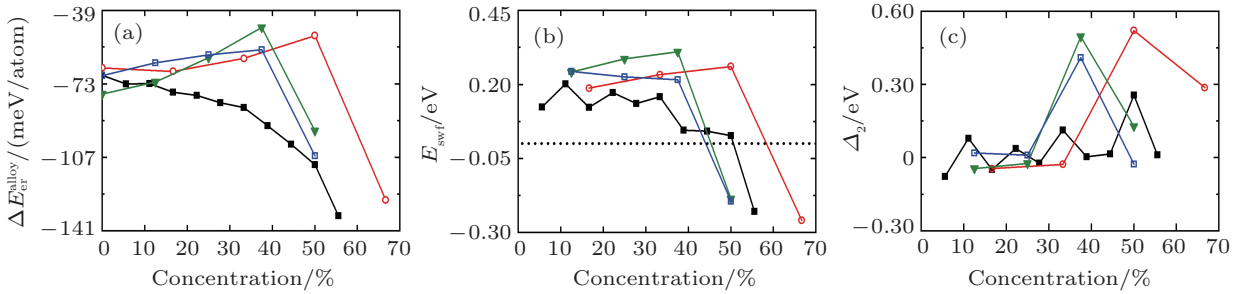

Fig. 2. Plots of relative energy release $\Delta E_{\rm er}^{\rm alloy}$, step wise formation energy $E_{\rm swf}$, and the second-order finite difference of the total energy Δ_2 *versus* doping concentration, with solid green down triangle, empty blue square, empty red circle, and solid black square denoting the alloying of BHS-2T, TRP-1T, SRT7-1T, and SRT19-3T germanenes supported on Al (111), respectively.

In Fig. 2, the calculated change in energy $\Delta E_{\rm er}^{\rm alloy}$ determined by formula (2) is also shown. For the SRT19 model, the alloying would continuously reduce the $\Delta E_{\rm er}^{\rm alloy}$ to lessen its fabrication possibility due to the formation of the isolated atoms. However, the SRT7-1T, TRP-1T, and BHS-2T are different. Their $\Delta E_{\rm er}^{\rm alloy}$ values would increase with the alloying process proceeding until the doping concentrations reach the corresponding critical values. Beyond the critical concentrations, their $\Delta E_{\rm er}^{\rm alloy}$ values decrease abruptly, turning to be obviously lower than the reference energy $E_{\rm er}^{\rm HL}$, thus significantly suppressing their formation. In our study, we also estimate the relative stabilities of the alloyed configurations with the alloying process proceeding. According to the calculated $E_{\rm swf}$ values shown in Fig. 2(b), the alloying could occur, starting from the undoped germanene sheets until they reach the critical doping concentrations. For a given structural model, the relative stability increasing with the augment of the doping concentration could be estimated by the second order finite difference of total energy Δ_2 as defined below:

$$\Delta_2(N) = E_{N+1} - 2E_N + E_{N-1}, \tag{4}$$

where E_{N+1}, E_N, and E_{N-1} are the total energy of the alloy configurations containing $N+1$, N, and $N-1$ Al atoms, respectively. The calculated data provided in Fig. 2(c) accord with the $\Delta E_{\rm er}^{\rm alloy}$ values shown in Fig. 2(a). Attributed to the abrupt drop of the $\Delta E_{\rm er}^{\rm alloy}$ values beyond the corresponding critical values, the alloy configurations with the critical doping concentrations gain relative stabilities, suggesting that they are the dominant Al–Ge alloy structures providing that the corresponding alloying processes could occur in experiment. For these relatively stable configurations, we calculate the charge populations of the protruded Ge atoms by using the Bader

charge analysis,[36,37] which are found to gain ∼ 1.4 e on average from their surrounding Al atoms. For comparing with the experimental observations, we also simulate their STM images and their counterpart germanene models without Al doping. Considering the STM study reported by Derivaz *et al.*,[14] the images are simulated for the +1.3 V bias by following the Tersoff and Hamann approach.[38–40]

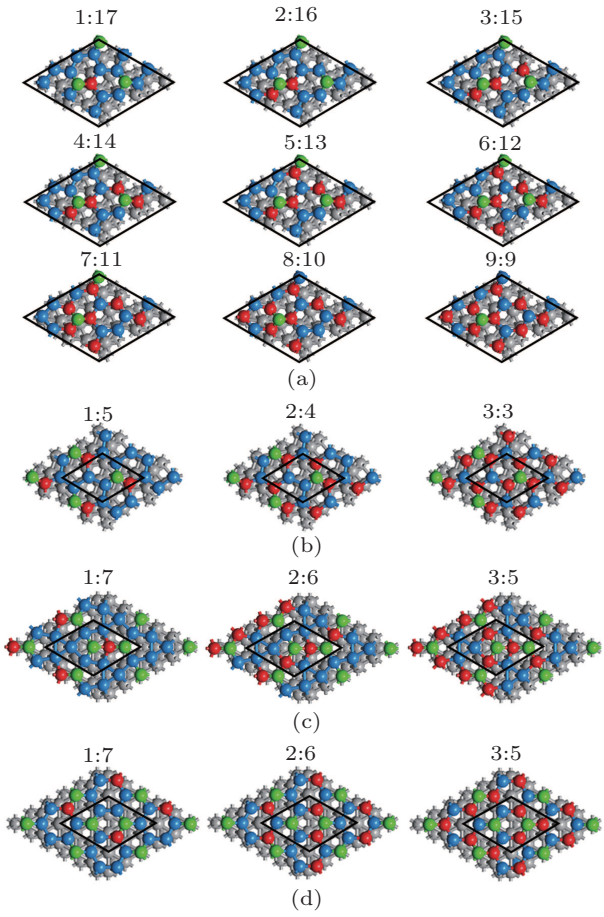

Fig. 3. Alloy configurations with positive formation energy E_{swf} corresponding to (a) SRT19-3T , (b) SRT7-1T, (c) TRP-1T, and (d) BHS-2T germananes supported on Al (111). The Al:Ge ratio of numbers of Al and Ge atoms in unit is also provided. The black rhombuses are the periodic units used in calculation. Grey, blue, green, and red sphere denote Al atom in substrate, Ge atom in the basal plane of the 2D sheet, Ge atom protruded upward which can be seen in STM image of the 2D sheet, and Al atoms doped in basal plane of the 2D sheet, respectively.

The simulated STM images are shown in Fig. 4. For the undoped germanene models, the BHS-2T model has the honeycomb-like bright-spot pattern while all the other ones own triangularly arranged bright spots. For the relatively stable alloy species, the TRP model shows the honeycomb-like bright-spot pattern also. The distance between the nearest neighboring bright spot is 8.47, 4.89, 7.15, and 7.47 Å for the undoped TRP, BHS, SRT19, and SRT7 models, and 4.89, 4.89, 12.31, and 7.47 Å for the corresponding stable alloy species, respectively. Comparing with the experimental studies, the models having STM images as either the honeycomb-like pattern with ∼ 4.89 Å as the distance between the nearest neighboring bright spots or the triangular pattern with ∼ 8.47 Å or 7.47 Å of the distances could be regarded as the configuration candidates. The SRT19 model for both the undoped germanene and alloyed germanene could not reproduce the experimentally observed STM images, which can be then ruled out as the structural candidate for germanene model on Al (111) surface. In addition, the structural model BHS-1H was previously proposed as the structural candidate also.[16,17,35] This model has the triangularly arranged bright spots in the simulated STM image with the ∼ 8.47 Å distance between neighboring spots. Interestingly, the potential structural candidates as the BHS models and the TRP configurations have the same number of atoms in the unit cell. The BHS-1H and TRP-1T models would immediately change to the BHS-2T and TRP-2T models even at the beginning of the alloying. Thus, one could only observe the honeycomb-like hexagonal bright-spot pattern, providing only the Al–Ge alloy sheets grow on Al (111)-(3 × 3), which would however conflict with the experimental studies. The experimental STMs also support the BHS-1H and TRP-1T models as structural candidates besides the BHS-2T and TRP-2T. So, the germananes without alloying could not be ruled out. In our study, we find that the undoped BHS-1H, BHS-2T, SRT7-1T, and TRP-1T only differ by less than 19 meV/atom in total energy. So, they probably have roughly equal chance to be fabricated in experiment. As shown in Fig. 2(a), the alloying of these models slightly increase their ΔE_{er}^{alloy} in the range of the low doping concentration, favoring the relatively stable Al_3Ge_3 SRT7-1T, Al_3Ge_5 BHS-2T, and Al_3Ge_5 TRP-2T to grow in experiment from the point of the view of direct fabrications with isolated Al and Ge atoms. In addition, we perform the constant-energy first-principles molecular dynamics simulations (FPMD) of the relatively stable Al–Ge alloy species supported on Al (111) surface after heating them up to 800 K. Each simulation lasts 5 ps in time steps of 0.5 fs. In order to reduce the limitation of the structural distortion due to the periodic conditions, the (3 × 3)-sized supercell for each sheet structure is used in the study, for which the structural unit to mimic the Al (111) substrate is also enlarged accordingly. Due to the intensive computing loading, we use the 4-layer slab with the bottom one fixed to mimic the bulk properties for the Al (111) surface. The in-plane lattices are ∼ 25.4 Å in spacing for the supercells containing 396 atoms for each of the BHS- and TRP-type geometries, while they are ∼ 22.0 Å for the supercell having 306 atoms for the SRT7-type configuration. The lattice perpendicular to the sheet is chosen to 21.0 Å in spacing. The structures obtained at the end of the simulations is optimized at 0 K, which are found to converge to the ideal stable Al–Ge alloy sheets without energy barriers. Our FPMD simulations

suggest that these Al–Ge alloy sheets are probably stable at a temperature of 360 K that is used in the experimental studies of germanene grown on the Al (111) surface,[14,16] showing the possibility of their formations in experiment.

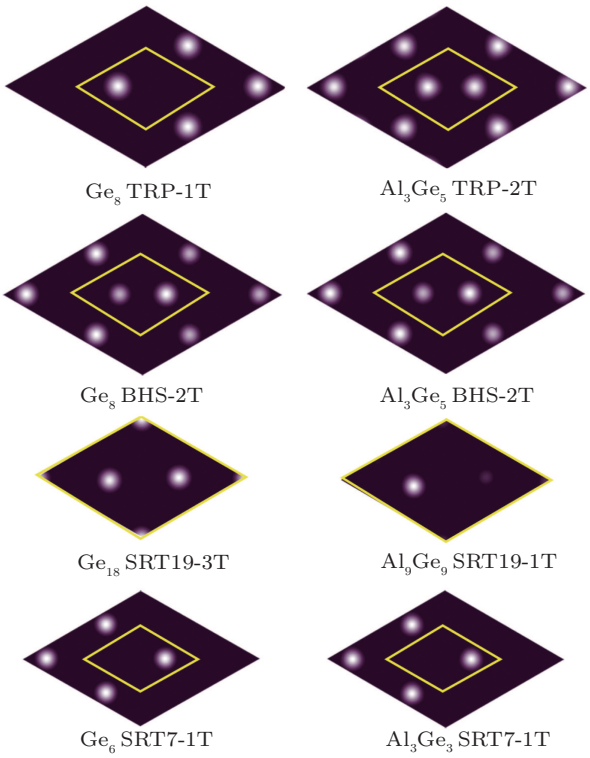

Fig. 4. STM images simulated at +1.3-V bias of pure germanenes TRP-1T, BHS-2T, SRT19-3T, and SRT7-1T and the corresponding stable alloy species Al_3Ge_5 TRP-2T, Al_3Ge_5 BHS-2T, Al_9Ge_9 SRT19-1T, and Al_3Ge_3 SRT7-1T supported on Al (111), with yellow rhombuses representing periodic units used in calculation.

3.2. Interface effects on germanene alloying

On the pristine Al (111) surface, the HL is calculated to be the ground state though it is not supported by the experimental STM studies. However, the buckled superlattices such as the TRP, BHS, and SRT7 configuration being less stable judged from the energy analysis can be used to simulate the experimental STM images. As indicated by previous studies, such a discrepancy could be reduced by the interface engineering.[35] Considering the previous results of the surface and near-surface alloying studies of aluminum surface,[41–46] we would like to say that the surface alloying can be one of the potential interface engineering techniques. In addition, the Al_2Ge surface alloy analogous to the Ag_2Ge surface alloy[44–46] was previously calculated to be favorable based on energy analysis[35] (see Fig. 5 for the structural illustration). So, we would also like to use the Al (111) surface alloy to estimate whether the surface engineering could make SRT, TRP, and BHS models to gain priorities in energy to facilitate their fabrications?

Again, applying the structural models to the Al_2Ge surface alloy, we then carefully optimize the structures with the supporting surface under different matching conditions. For the SRT19 configuration (see Fig. 1 for illustration), it can only match the Al_2Ge with the supercell containing 1188 atoms, which consume too computing time to be used as our computing resource. In addition, no experimental indication is reported that this alloy can be fabricated on Al (111) surface. So, we do not calculate its alloying on the Al_2Ge surface alloy. As to the SRT7 model, a supercell as the 3×3-sized SRT7 supercell referring to the repeated 6-atom unit on Al (111) needs to match the Al_2Ge surface alloy, thus containing 432 atoms in the calculated system. Owing to the limitation of our computing resource, we just repeatedly transfer the corresponding configurations obtained for this model supported on the pure Al (111) surface to construct the 3×3-sized configurations, which are then located on Al_2Ge surface alloy for structural optimization. To facilitate the comparison with the cases of using the Al (111) surface as support, we discuss the alloying process of the SRT7-(3×3) sheet on Al_2Ge by using the doping concentration of the 6-atom fragment. The optimized configurations for the undoped germanenes are illustrated in Fig. 5.

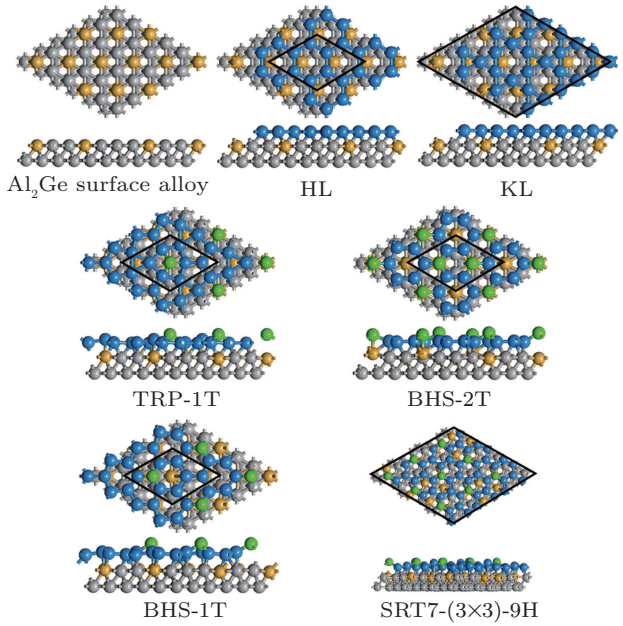

Fig. 5. Schematic illustrations of structural models of germanenes grown on Al_2Ge surface alloy along with the configuration of Al_2Ge itself. Only two top layers of substrate are shown. Black rhombuses are periodic units used in calculation. Grey, blue, green, and yellow spheres are Al atom in substrate, Ge atom in basal plane of the 2D sheet, Ge atom protruded upward which can be seen in STM image of the 2D sheet, and Ge atoms doped in Al_2Ge surface alloy, respectively.

The HL, KL, BHS, and TRP models keep their structural characteristics while the SRT7 is found to have severer distortion. As shown in Fig. 5, the Ge above the doped Ge in the Al_2Ge surface alloy is lowered downward, which in turn makes its next-nearest Ge atoms in the SRT7 sheet pop up. Finally, there are 9 Ge atoms at the H-like hollow sites protruded upward in the SRT7-(3×3) supercell. According to

these structures, we investigate their alloying. Again, the HL and KL are found to have negative E_{swf} values to suppress their alloying. The studied E_{swf} and ΔE_{er}^{alloy} are shown in Fig. 6.

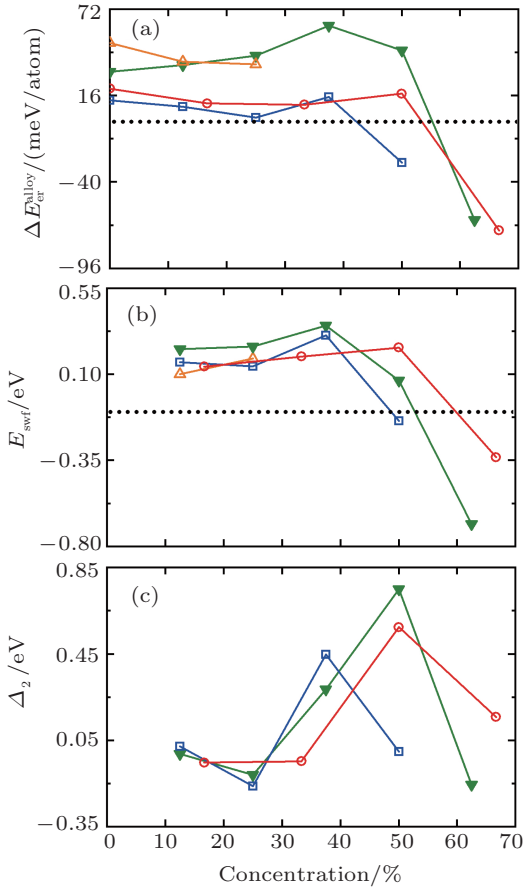

Fig. 6. Plots of relative energy release ΔE_{er}^{alloy}, step wise formation energy E_{swf}, and second order finite difference of total energy Δ_2 *versus* doping concentration, with empty yellow up triangle, solid green down triangle, empty blue square, and empty red circle denoting alloying of the BHS-1H, BHS-2T, TRP-1T, and SRT7-1T germanenes supported on Al_2Ge, respectively.

In the calculation of ΔE_{er}^{alloy} by using formula (2), the pure HL germanene supported on Al_2Ge is selected as the reference. Judged from the E_{swf}, the critical concentrations are Al:Ge = 3:3 for SRT7, 3:5 for TRP, and 4:4 for BHS configurations, respectively. Unlike the cases supported on the pure Al (111) surface, only BHS-2T model has the ΔE_{er}^{alloy} to monotonically increase in the low doping concentration range to enhance its energetic priority for fabrication. The ΔE_{er}^{alloy} value for each of the BHS-1H, TRP-1T, and SRT7-(3 × 3)-9H model are found to decrease at the beginning of alloying (see Fig. 6(a)). Providing the formation starts from the free-standing Al and Ge atoms, the decrease of ΔE_{er}^{alloy} means that the corresponding fabrications would be suppressed to a certain extent. Providing the pure BHS-1H, TRP-1T, and SRT7-(3 × 3)-9H structures each are first fabricated on an Al_2Ge surface alloy, the corresponding alloy sheets may also be synthesized as low-lying isomers because the presence of Al at the beginning of the alloying only sacrifices less than 14 meV/atom of the corresponding ΔE_{er}^{alloy}. Also, judged from the positive E_{swf} presented in Fig. 6(b), the alloying process could occur starting from the undoped sheets. The E_{swf} would turn to be negative thus suppressing the alloying when doping density is beyond the critical doping concentration. The alloyed configurations with the positive E_{swf} values are shown in Fig. 7 (the structures with negative E_{swf} values are provided in Fig. A4 in Appendix A).

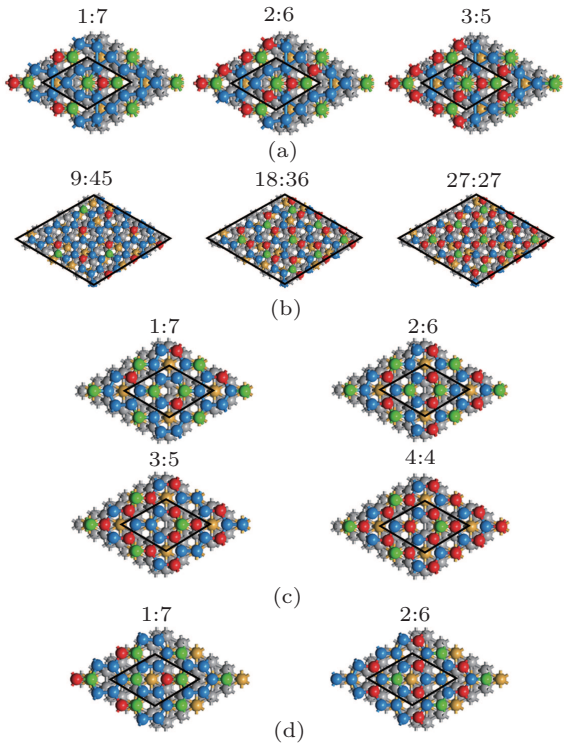

Fig. 7. Alloy configurations with positive formation energy E_{swf} corresponding to (a) TRP-1T, (b) SRT7-(3 × 3)-9H, (c) BHS-2T, and (d) BHS-1H germananes supported on Al_2Ge. The Al:Ge ratio between the numbers of Al and Ge atoms in the unit is also provided. Black rhombuses represent periodic units used in calculation. Grey, blue, green, yellow, and red sphere denote Al atom in substrate, Ge atom in basal plane of the 2D sheet, Ge atom protruded upward which can be seen in STM image of the 2D sheet, Ge atoms doped in the Al_2Ge surface alloy, and Al atoms doped in basal plane of the 2D sheet, respectively.

As shown in Fig. 6, the interface interaction engineering brings effects to the Al–Ge alloy sheets. Unlike the case of Al–Ge sheet on Al (111), the BHS-1H could now remain for the $AlGe_7$ and Al_2Ge_6 alloys, which would change into the BHS-2T model starting from the Al:Ge = 3:5 concentration. The TRP model acts similarly for the case of using Al (111) as support. On the Al_2Ge surface alloy, the TRP model would also immediately change from TRP-1T to TRP-2T at the beginning of the alloying. For the BHS-2T, it could remain the structural characteristics for $AlGe_7$ and Al_2Ge_6 alloy sheets, which would however become BHS-1T configuration for Al_3Ge_5 and Al_4Ge_4 sheet. Here, BHS structure could hold one more Al dopant as compared with its alloying process supported on Al (111). In the 1:5 doping configuration of the SRT7-(3 × 3) model, the charge re-distribution induced

by the doped Al results in 6 Ge atoms to become dim in our simulated STM, which has only 3 Ge atoms to be clearly seen in the STM image though the structural characteristics almost remain. Similar phenomena were previously found also in our theory-experiment joint studies of the single Cu, Ag, and Au atom adsorption on Si (111)-(7 × 7) surface.[39,40] Due to less states close to the Fermi level, some of the atoms may not be seen in the STM studies though their heights above the surface are obvious. Here, we calculate the partial densities of states (PDOSs) of these 6 Ge atoms (see Fig. A6 in Appendix A). It is true that these Ge atoms have less states in the energy windows close to Fermi level, which cannot be seen in the STM images simulated under both positive and negative bias. For the 2:4 and 3:3 concentration, our structural optimizations give the SRT7-(3 × 3)-9T configurations with one Ge protruded upward in each 6-atom structural fragment which has the same structural characteristics as those of the SRT7-1T model supported on Al (111). By calculating the second order finite difference of total energy by using formula (4), we obtain the relative stabilities of the alloyed configurations, which are shown in Fig. 6(c). Due to the abrupt drop in $\Delta E_{\rm er}^{\rm alloy}$ after the critical doping concentrations, the Al_4Ge_4 BHS-1T, Al_3Ge_5 TRP-2T, and $Al_{27}Ge_{27}$ SRT7-(3 × 3)-9T gain superiorly relative stabilities. In addition, we would like to mention the Al_3Ge_5 BHS-1T. Though it has the biggest $\Delta E_{\rm er}^{\rm alloy}$, it however has no difference in the simulated STM images as compared with the Al_4Ge_4 BHS-1T. Hereafter, we would like to concentrate on discussing the relatively stable species Al_4Ge_4 BHS-1T. In the Al_4Ge_4 BHS-1T, the protruded Ge atom gains 1.24 e charge more from the Al dopants than the corresponding Ge atom in the undoped BHS configuration.

Its height is found to remain almost unchanged. Comparing with the undoped TRP-1T structure, the protruded Ge atom at the Ge_6 center in the Al_3Ge_5 TRP-2T gains 0.89 e and lowers down in height by 0.5 Å while the Ge atom at the vertex shared by three fused Ge_5 pentagons now pops up and gains 1.20-e charge. In the $Al_{27}Ge_{27}$ SRT7-(3 × 3)-9T, the protruded Ge atom obtains ∼ 1.21 e from the doped Al atoms.

Besides the alloy geometries, the interface interaction engineering also affects the energy sequence of the germanene sheets grown on Al_2Ge surface alloy. Unlike the case of Al–Ge alloy sheets on Al (111), the $\Delta E_{\rm er}^{\rm alloy}$ values shown in Fig. 6(a) keep positive until they reach their corresponding critical values. For the 2D configurations shown in Fig. 5, the BHS-1H is found to have the largest $E_{\rm er}$ calculated from formula (1), which is taken as the $E_{\rm er}$ value of the ground state of pure germanene. The interface engineering effect makes the HL (the energetically preferred configuration on Al (111) surface) have 50 meV/atom less favorable in energy to suppress its fabrication in experiment. The KL is also not preferable as judged from the calculated $E_{\rm er}$ energy, which is 93 meV/atom lower than the BHS-1H. The BHS-2T, SRT7-(3 × 3)-9H, and TRP-1T have 19, 30, and 37 meV/atom lower $E_{\rm er}$, respectively. As the corresponding alloying studied in Fig. 6(a), only BHS-2T model has the increased $\Delta E_{\rm er}^{\rm alloy}$ at the beginning of alloying and thus facilitating the corresponding synthesis. The $\Delta E_{\rm er}^{\rm alloy}$ value reaches 45 meV/atom at the critical doping concentration. Also, the $\Delta E_{\rm er}^{\rm alloy}$ value of the stable Al_4Ge_4 BHS-1T is 28 meV/atom (30 meV/atom) higher than the $Al_{27}Ge_{27}$ SRT7-(3 × 3)-9T (Al_3Ge_5 TRP-2T) relatively stable species, which favors the formation of Al_4Ge_4 BHS-1T in view of the fabrication with isolated atoms.

Figure 8 shows the simulated STM images for the stable Al_4Ge_4 BHS-1T, Al_3Ge_5 TRP-2T, and $Al_{27}Ge_{27}$ SRT7-(3 × 3)-9T and their corresponding structural models for the undoped germanenes. The BHS-1H model for pure germanene and the Al_2Ge_6 alloy sheet are also simulated in Fig. 8 for the comparison study. The shortest spot–spot distance is 4.89 Å (8.47 Å) for the hexagonally (triangularly) arranged bright spots of the BHS (TRP) configuration, theses results are in accordance with the experimental STM images.[14,16,17,20] In the STM image of the SRT7-(3 × 3)-9H for pure germanene, the bright spots are clustered into 3-spot triangles with the 7.20-Å long sides. The 3-spot triangles are then triangularly separated from each other by a center–center distance of 12.93 Å between neighboring triangles. This results in the distances between neighboring bright spots in its STM image to be 7.20, 7.43, and 7.79 Å, which need verifying experimentally. Differently, in the STM image of the relatively stable alloy species $Al_{27}Ge_{27}$ SRT7-(3 × 3)-9T, the bright spots are uniformly arranged in the triangular pattern with a 7.47-Å spot–spot distance between neighboring spots. Such a triangular pattern can be regarded as the 3 × 3 mesh of bright spots with each of them in a rhombic fragment (see the illustration of the red rhombus in Fig. 8), which looks similar to the experimental STM image proposed for the SRT7-1T unit.[17,18] Providing the experimental studies are carried out under well-controlled conditions without excess Al atoms to alloy the germanene, the energetically preferred BHS-1H can be probably fabricated in experiment, while the 19-, 30-, and 37-meV/atom less-stable BHS-2T, SRT7-(3 × 3)-9H, and TRP-1T may also be grown as low-lying isomers. However, if there are Al atoms involved in experimental fabrications, the Al_4Ge_4 BHS-1T turns to be the most stable one in the alloy species. The relatively stable species $Al_{27}Ge_{27}$ SRT7-(3 × 3)-9T and Al_3Ge_5 TRP-2T are the low-lying isomers of the alloy sheets. For the Al_2Ge_6 BHS-1H, it cannot be preserved providing enough Al atoms are involved in the reaction because it

would evolve into the Al_3Ge_5 BHS-1T configuration to release $\sim$ 25-meV/atom energy. Again, we perform 5-ps-long constant energy FPMD simulations of the relatively stable Al–Ge alloy species supported on the Al_2Ge surface alloy after heating them up to 800 K. The structures obtained at the end of the simulations are then fully optimized at 0 K, which are found to converge to the ideal relatively stable Al–Ge sheet geometries. The FPMD studies suggest their stabilities at a temperature of 360 K adopted in experimental studies,[14,16] indicating that the relatively stable Al–Ge alloy species may have a chance to be fabricated in experiment.

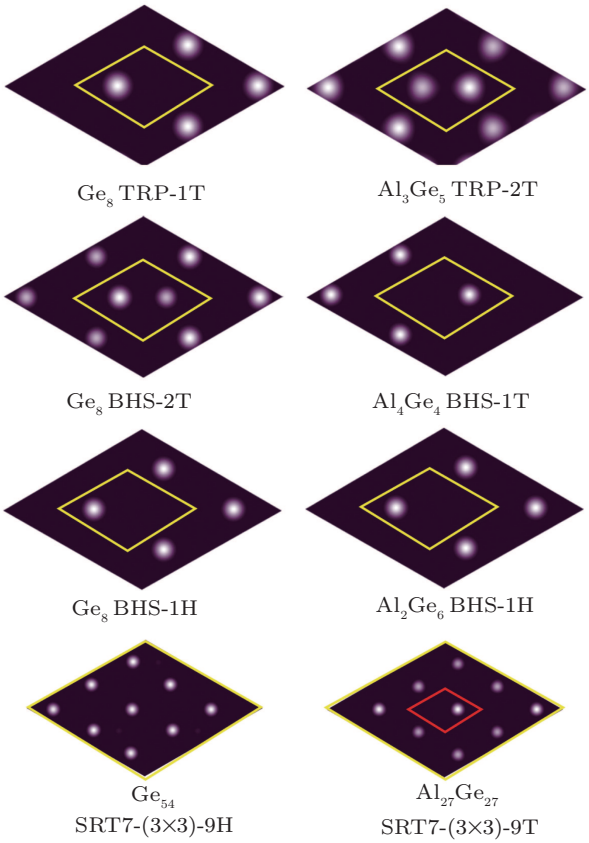

Fig. 8. STM images simulating +1.3-V bias for Ge_8 TRP-1T and its alloy sheet Al_3Ge_5 TRP-2T, Ge_8 BHS-2T, and Al_4Ge_4 BHS-1T, Ge_8 BHS-1H and Al_2Ge_6 BHS-1H, and Ge_{54} SRT7-(3 × 3)-9H, and $Al_{27}Ge_{27}$ SRT7-(3 × 3)-9T supported on Al_2Ge. In image of $Al_{27}Ge_{27}$ SRT7-(3 × 3)-9T, red rhombus corresponds to the smallest repeated unit of the bright-spot pattern. The yellow rhombuses denote periodic units used in calculation.

3.3. Discussion

On the pure Al (111) surface, the HL geometry is the most stable one according to the energy analysis. The KL is the 47-meV/atom less-stable first low-lying isomer. However, none of the previous experimental STM studies suggested their fabrications. The SRT7-1T, TRP-1T, BHS-2T, and BHS-1H have the simulated STM images consistent with the experimental images, which are however 66-, 69-, 78-, and 85-meV/atom less stable than the HL geometry judged from our energy analyses. The alloying each of HL sheet and KL sheet is found to be endothermic, thereby keeping their pure germanene structures unchanged, while it is exothermic to alloy the SRT7, TRP, and BHS geometry till their critical doping concentrations are reached, respectively. So, the SRT7, TRP, and BHS models cannot remain their pure germanenes as they are, if the alloying can occur, which would evolve into the relatively stable alloy species Al_3Ge_3 SRT7-1T, Al_3Ge_5 TRP-2T, and Al_3Ge_5 BHS-2T correspondingly as suggested by our second order finite difference analyses of the total energy. However, they are still less stable in energy than the pure HL sheet, and found to be the 51-, 57-, and 47-meV/atom less-stable low-lying isomers. Our simulated STM images of the relatively stable alloy species are consistent with the experimental images also. In the alloyed sheets, the BHS-1H model cannot be preserved, which will evolve into the BHS-2T configuration at the beginning of alloying. The structural transition between BHS-1H and BHS-2T as indicated experimentally[16] cannot be stood once the alloying starts, though it can for the pure sheet structures. Furthermore, both of the alloyed Al_3Ge_5 TRP-2T, and Al_3Ge_5 BHS-2T are found to have two bright spots at the top sites (see Fig. 4), none of which coincides with the switch between the pattern with one bright spot per unit and the pattern with two bright spot per unit observed on experiment.[16] The SRT7-1T has one bright spot per unit which however matches the Al (111)-$\left(\sqrt{7}\times\sqrt{7}\right)$ (19.1°) surface[17,18] instead of the Al(111)-(3 × 3) surface used in the structural transition study.[16] So, we would like to say that none of the alloyed structures themselves for all of the previously reported experimental results can be stood. The well-controlled experimental conditions may help grow either pure or alloyed germanene sheets. However, the calculated ground state is of the HL structure for the sheets grown on Al (111). The energy difference between the ground state and its first low-lying isomer is 66 meV/atom (the Ge_6 SRT7-1T geometry) providing only pure germanene sheets are grown, and 47 meV/atom (the Al_3Ge_5 BHS-2T alloy sheet) providing the germananes are alloyed. To some extent, such energy differences can suppress the growth of the bulked superlattice geometries such as the SRT7, TRP, and BHS structures. This in turn supports the HL growth on an ideal Al (111) surface, which however, is in conflict with the experimental result.

There are probably some detailed experimental conditions that can affect the germanene growing on an aluminum substrate, which we could not say on the basis of what we know from the existing experimental papers. The detailed theory-experiment joint studies are still needed to clarify the crucial reason to facilitate the investigation of cheap substrate material for fabricating the 2D materials. Here, considering the fact that the metal surface can be engineered through the technique known as surface alloying,[35,41–46] we try to

use the surface alloy of Al (111) as a tentative method to see whether the germanene models meeting the experimental observations can gain energetic priorities to facilitate their large-quantity fabrications. The Al_2Ge surface alloy configuration analogous to the Ag_2Ge surface alloy[44–46] is exothermic for formation.[35] Interestingly, the ground state is BHS-1H providing only pure germanene can be grown, which is 50 meV/atom more favorable in energy than HL. Thus, the growth of HL germanene structure would will be obviously suppressed . The BHS-2T now turns to be the first low-lying isomer that is only 19-meV/atom less stable. The SRT7 and TRP geometries are found to be 30- and 37-meV/atom less stable, respectively. Again, HL and KL are still undoped alloys. Though the calculated $E_{\rm swf}$ provided in Fig. 6(b) supports that the occurrence of alloying starts from the BHS, SRT7, and TRP germanene in the low doping concentration range, only the BHS-2T model is found to have the increased $\Delta E_{\rm er}^{\rm alloy}$ in Fig. 6(a), favoring its growth providing the structure is fabricated with isolated Al and Ge atoms. For each type of models, the second order finite differences of total energy suggest that the Al_4Ge_4 BHS-1T, Al_3Ge_5 TRP-2T, and Al_3Ge_3 SRT7-1T are the relatively stable species. So, if the experiments can be well-controlled, both the pure germanene and the alloyed germanene will be able to be fabricated, depending on the experimental conditions.

The structural transition between them can occur.[16,35] If Al atoms that are present in experimental conditions are involved in the fabrication reactions or alloy the beforehand prepared germanenes, the BHS, SRT7, and TRP models will evolve into the relatively stable alloy species, for which case the simulated STM images are consistent with the experimental images. However, the structural transition observed in experiment cannot occur among the relatively stable alloy species. So, the pure germanenes and the alloyed sheets could have the chance to be fabricated in the well-controlled experimental studies.

In Fig. 9, the charge accumulation and depletion are investigated for the selected typical structures, which are the ground states of pure germanenes on the Al (111) and Al_2Ge surface alloy and the most stable alloyed sheets supported on these substrates, respectively. Such charge transfer analyses for the other studied structures are provided in Figs. A5 and A7 in Appendix A. For the sheet structure supported on substrate, the charge density of the structural fragments such as the sheet itself ($D_{\rm 2D}$) and the substrate ($D_{\rm substrate}$) with the corresponding geometries like those in the optimized structure of the sheet supported on substrate, and the density of the sheet supported on substrate ($D_{\rm 2D/substrate}$) is first calculated. Then, the charge transfer is estimated by subtracting the $D_{\rm 2D}$ and $D_{\rm substrate}$ from the $D_{\rm 2D/substrate}$. As shown in Fig. 9, the charge accumulation between the sheet and substrate and the charge depletion at the sheet and the top layer of substrate suggest that the interface interaction is covalent-like chemical interaction. Also, the protruded Ge atoms in the sheet do not directly develop chemical bonds with the substrate. In order to estimate the strength of the interface interaction, we calculate the corresponding adhesive energy from

$$E_{\rm adhesive} = \frac{E^0_{\rm 2D} + E^0_{\rm substrate} - E_{\rm 2D/substrate}}{S}, \tag{5}$$

where the $E_{\rm 2D/substrate}$ is the total energy of the optimized 2D geometry supported on the substrate, $E^0_{\rm 2D}$ and $E^0_{\rm substrate}$ are the energies calculated for the isolated structural fragments of the 2D structure and the substrate with the geometries of the optimized 2D/substrate material, and S is the area of the 2D sheet. The calculated data are presented in Table 1, indicating the weak chemical bonding between the sheet and the substrate. The surface alloy slightly weakens the interface interaction to turn the buckled germanene superlattices such as the BHS structures preferable, suggesting that the interface engineering acts as an effective method to facilitate the large quantity fabrication of germanene-based sheets.

Table 1. Calculated adhesive energy (in units of meV/Å^2) between 2D sheet and substrate with Ge_n and Al_mGe_n corresponding to unit of pure and alloyed 2D sheet, respectively.

Structure	Al (111)	Al_2Ge	Structure	Al (111)	Al_2Ge
Ge_6 HL	114	101	Ge_8 BHS-2T	92	85
Ge_{27} KL	107	92	Al_3Ge_5 TRP-2T	121	107
Ge_8 BHS-1H	83	81	Al_3Ge_5 BHS-2T	104	–
Ge_8 TRP-1T	99	9	Al_4Ge_4 BHS-1T	–	– 101
Ge_6 SRT7-1T	9	–	Al_3Ge_3 SRT7-1T	113	–
Ge_{54} SRT7-(3 × 3)-9H	–	78	$Al_{27}Ge_{27}$ SRT7-(3 × 3)-9T	–	104

In addition, the calculated $E_{\rm adhesive}$ ranges from 78 meV/Å^2 to 121 meV/Å^2 to show the possibility for the isolations of the fabricated sheets. However, all of the studied alloy sheets are found to break during the structural optimizations after isolating them from the substrate which plays a crucial role in stabilizing the 2D structures. For the pure

germanene structures, the HL, BHS-1H, BHS-2T, and SRT7-1T germanene structures will immediately converge to the well-known ground state of the free-standing germanene — the slightly buckled honeycomb structure, while neither the KL nor TRP-1T, however, is stable in the free-standing state. Though none of the corresponding isolated configurations is stable, the buckled superlattice of pure germanene and the alloy sheets supported on substrates may also have potential applications such as in helping anchor small catalyst particles through the enhanced reactivities of the well-separated protruded Ge atoms in the sheets, which are worth further studying experimentally and theoretically.

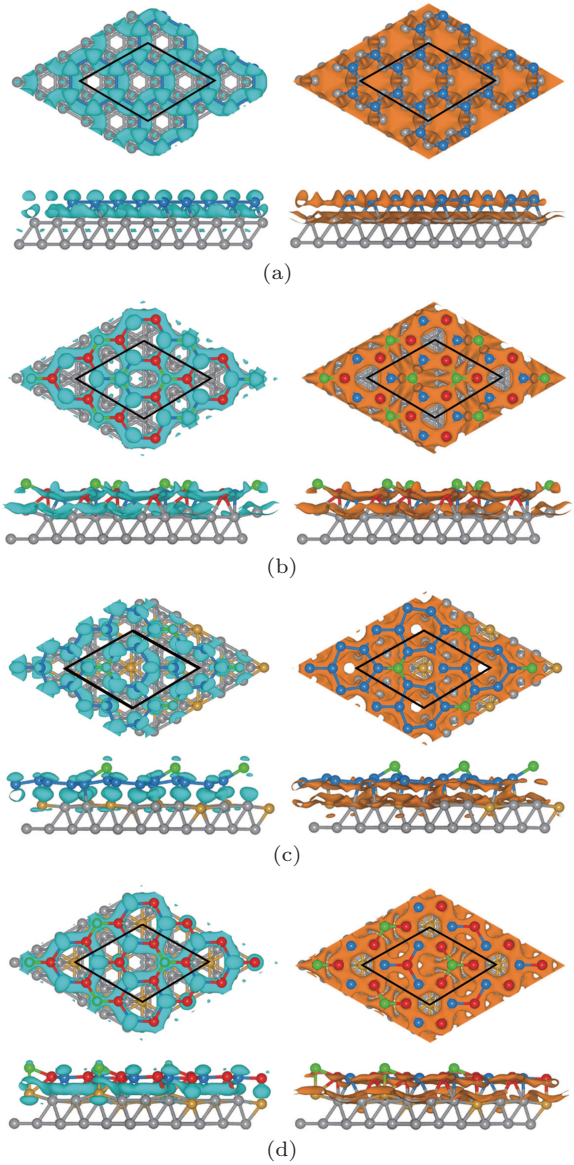

Fig. 9. Isosurfaces at 0.015 e/Å^3 for charge accumulation (cyan) in left panel and the charge depletion (orange) in right panel. Panels (a) and (b) are for pure germanane structure HL and stable Al_3Ge_5 BHS-2T supported on Al (111). Panels (c) and (d) are for pure germanene structure BHS-1H and the stable Al_4Ge_4 BHS-1T supported on Al_2Ge surface alloy.

In addition, we also estimate whether the hydrogenation could help achieve the stable isolated alloy sheet. For the alloy sheet supported on the substrate, the protruded Ge atoms are ready for hydrogen adsorptions. After that, more hydrogen atoms can be adsorbed on the Ge atoms which are the next nearest to the pre-hydrogenated ones in the Al_4Ge_4 BHS-1T structure and the Al_3Ge_3 SRT7-1T sheet, resulting in the configurations with the Ge atoms separated from each other by the Al atoms to be hydrogenated. Differently, in the Al_3Ge_5 BHS-2T structure, one of the protruded Ge atoms is surrounded by three neighboring Ge atoms, for which the pre-adsorbed H atom hinders these 3 neighboring Ge atoms from being futher hydrogenerated. In the Al_3Ge_5 TRP-2T structure, the hydrogen adsorptions at the protruded Ge atoms enlarges the Ge_3 triangle structural motif. More hydrogen atoms could be then adsorbed on the Ge atoms in this Ge_3 triangle structural motif to break the corresponding Ge–Ge bonds. After the structural optimizations of the supported alloy sheets, we then remove the corresponding substrates and carefully optimize all the sheet structures again. The optimized structures are then used to calculate the phonon spectra with the Phonopy code.[47] All hydrogenated alloy configurations but for the hydrogenated Al_3Ge_5 TRP-2T alloy sheet are found to have imaginary frequency modes, implying that they are unstable. As to the Al_3Ge_5 TRP-2T alloy sheet, we further evaluate its stability by carrying out the first-principles molecular dynamics simulation at room temperature. It is found to remains unchanged during our 5-ps long simulation, implying that it is stable.

4. Conclusions

Using density functional theory method, we have carefully studied the alloying process of germanenes supported on both Al (111) and its Al_2Ge surface alloy. The HL hexagonal lattice and the KL Kagome lattice keep pure germanene sheets, for which case the alloying with Al atoms is endothermic. All the other studied structural configurations would release energy in the range of low doping concentration to favor the alloying process accordingly. The stable BHS, TRP, and SRT7 geometry of the pure and alloyed germanenes supported on Al (111) and Al_2Ge surface alloy, except the SRT7 structure of pure germanene on Al_2Ge surface alloy, can re-produce the STM images as the structural candidates for the experimentally fabricated 2D sheets. On a pure Al(111) surface, the HL is the energetically favorable configuration with the KL as its first low-lying isomer. The BHS, TRP, and SRT7 germanene and their alloyed sheets are all larger than 40meV/atom less stable in energy to challenge their experimental syntheses. Using the surface alloy to illustrate the effect of interface engineering on the germanene growth, we show that the reduced activity of Al (111) surface facilitates the growing of the BHS,

TRP, and SRT7 structures, turning them superior in energy. Based on our second order finite difference analyses of the total energy, the relatively stable alloy species are found to be the Al_3Ge_5 BHS-2T, Al_3Ge_5 TRP-2T, and Al_3Ge_3 SRT7-1T on Al (111) while they are the Al_4Ge_4 BHS-1T, Al_3Ge_5 TRP-2T, and $Al_{27}Ge_{27}$ SRT7-(3×3)-9T on Al_2Ge surface alloy. Of the alloyed species, the Al_3Ge_5 BHS-2T on the Al (111) is the most stable structure from the point of the view of energetic stability and so is the Al_4Ge_4 BHS-1T on Al_2Ge surface alloy. For the pure germanenes, the HL and BHS-1H are the corresponding ground states on Al (111) and Al_2Ge, respectively. Though a structural transition between BHS-1H and BHS-2T model of pure germanenes is confirmed in previous theory–experiment joint study, such a kind of transition cannot be supported in the alloyed species. So, both the pure germanene and the alloyed germanene probably gain chances for their fabrications under well-controlled experimental conditions, which needs further comprehensively studying theoretically and experimentally.

Acknowledgment

Drs. Hongbo Wang and Jinghua Guo are highly appreciated for carefully reading our manuscript.

Appendix A: Supporting information

In order to better understand and explain the descriptions in the main text, some supporting figures are given in the following for references.

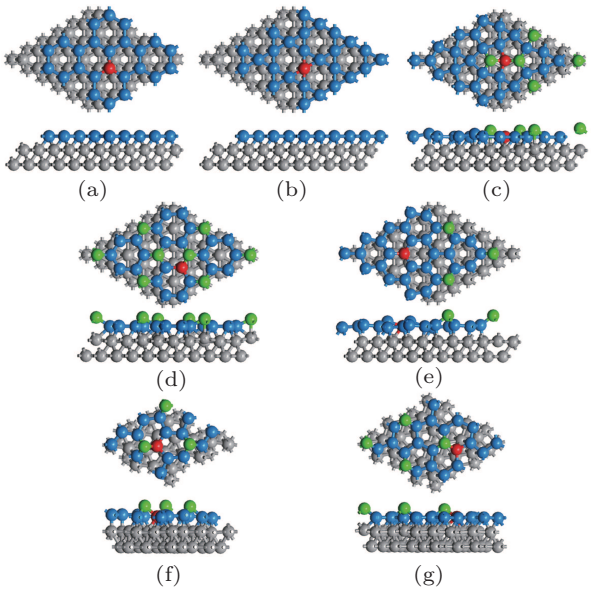

Fig. A1. Doping configurations of a single Al atom in 2D germanene models supported on Al (111) corresponding to (a) HL, (b) KL, (c) TRP-1T, (d) BHS-2T, (e) BHS-1H, (f) SRT19-3T, and (g) SRT7-1T structures. Grey, blue, green, and red spheres denote Al atoms in substrate, Ge atoms in basal plane of the 2D sheet, Ge atoms protruded upward which can be seen in STM image of the 2D sheet, and Al atoms doped in basal plane of the 2D sheet, respectively.

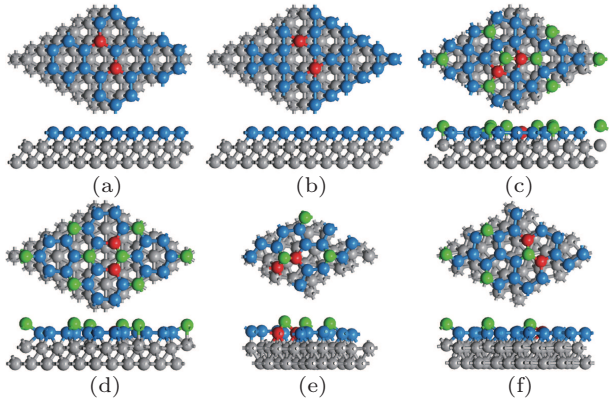

Fig. A2. Ground state configurations of two Al atoms doped in 2D germanenes supported on Al (111) corresponding to (a) HL, (b) KL, (c) TRP-1T, (d) BHS-2T, (e) SRT19-3T, and (f) SRT7-1T structures. Grey, blue, green, and red spheres denote Al atoms in substrate, Ge atoms in basal plane of the 2D sheet, Ge atoms protruded upward which can be seen in STM image of the 2D sheet, and Al atoms doped in basal plane of the 2D sheet, respectively.

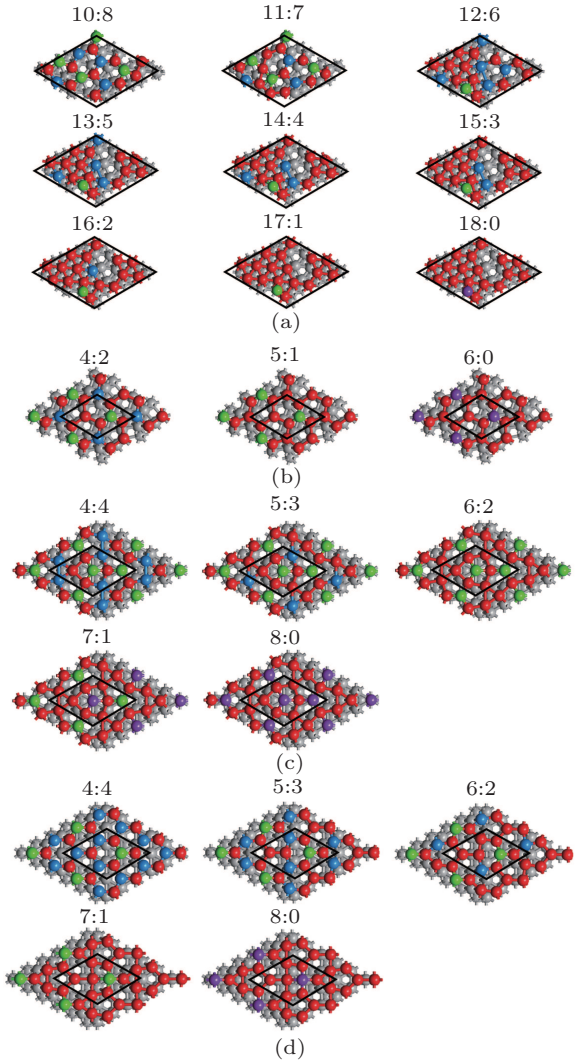

Fig. A3. Alloy configurations with negative formation energy E_{swf} corresponding to (a) SRT19-3T, (b) SRT7-1T, (c) TRP-1T, and (d) BHS-2T germananes supported on Al (111). Number ratio of Al and Ge atoms in unit Al:Ge is also provided. Black rhombuses represent periodic units used in calculations, and grey, blue, purple, green, and red spheres denote Al atoms in substrate, Ge atoms in basal plane of the 2D sheet, Al atoms protruded upward in the 2D sheet, protruded Ge atoms in the 2D sheet, and Al atoms doped in the basal plane of the 2D sheet, respectively.

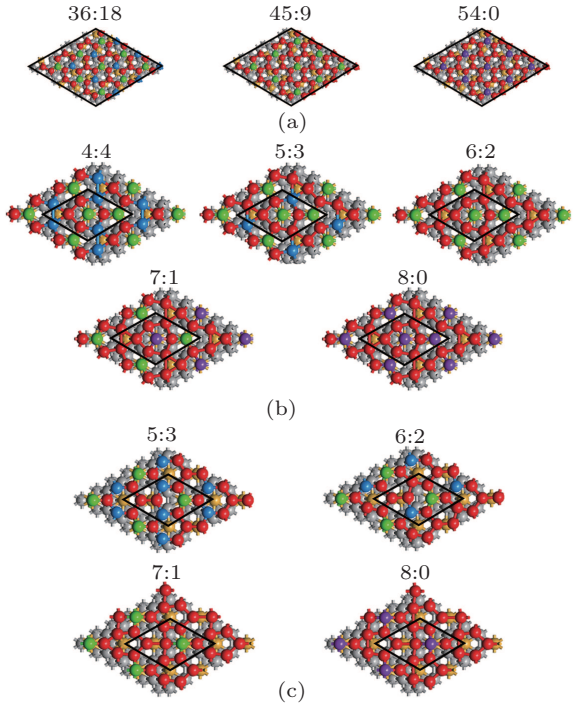

Fig. A4. Alloy configurations with negative formation energy E_{swf} corresponding to (a) SRT7-(3 × 3)-9H, (b) TRP-1T, and (c) BHS-2T germananes supported on Al_2Ge. Number ratio of Al and Ge atoms in unit Al:Ge is also provided. Black rhombuses represent the periodic units used in the calculations. The grey, blue, purple, green, and red spheres denote Al atoms in Al_2Ge substrate, Ge atoms in basal plane of the 2D sheet, Al atoms protruded upward in the 2D sheet, protruded Ge atoms in the 2D sheet, and Al atoms doped in the basal plane of the 2D sheet, respectively.

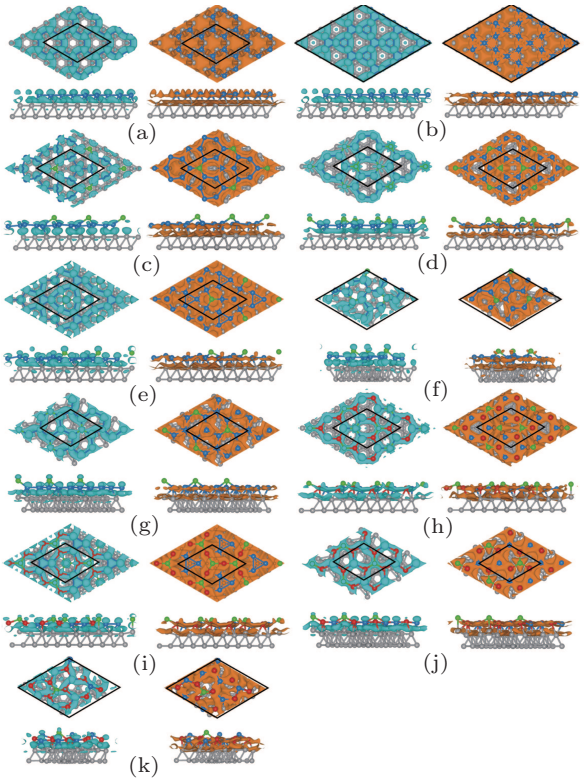

Fig. A5. Isosurfaces at 0.015 e/Å^3 for charge accumulation colored in cyan in the left panel and the charge depletion colored in orange in the right one indicating (a) HL, (b) KL, (c) BHS-1H, (d) BHS-2T, (e) TRP-1T, (f) SRT19-3T, and (g) SRT7-1T pure germanane structures supported on Al (111), respectively relatively stable alloy species (h) Al_3Ge_5 BHS-2T, (i) Al_3Ge_5 TRP-2T, (j) Al_3Ge_3 SRT7-1T, (k) SRT7-1T, and (k) Al_9Ge_9 SRT19-1T structures, respectively.

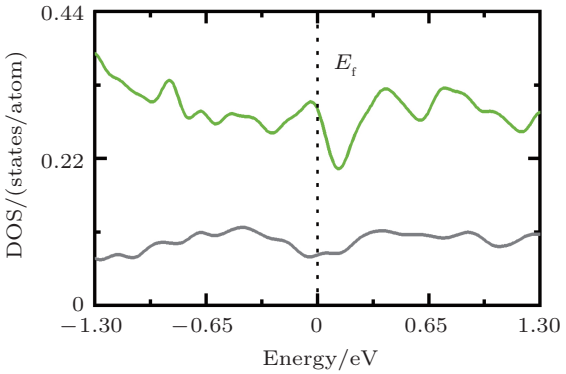

Fig. A6. Calculated PDOSs of Ge atom in Al_9Ge_{45} SRT7-(3 × 3) sheet. The green line is for protruded Ge atom that can be seen in the simulated STM image, and grey line is for protruded Ge atom that could not be seen in the simulated STM image.

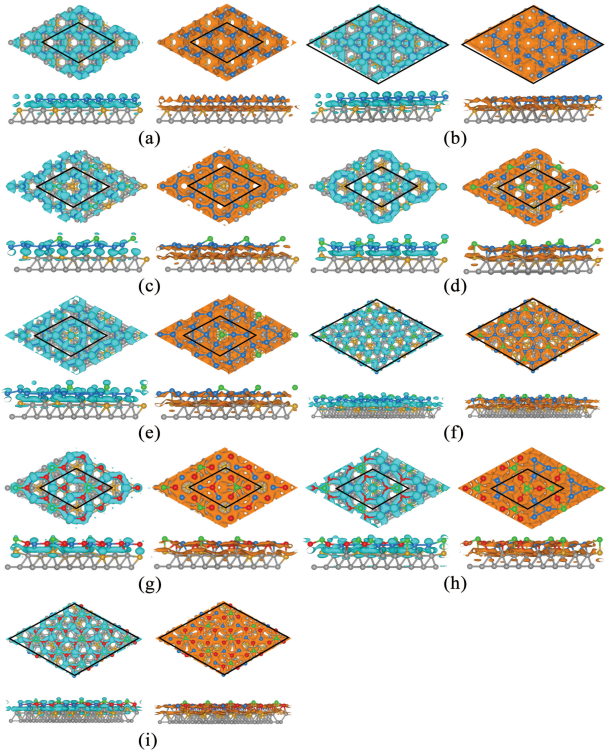

Fig. A7. Isosurfaces at 0.015 e/Å^3 for charge accumulation colored in cyan in the left panel and the charge depletion colored in orange in the right one indicating (a) HL, (b) KL, (c) BHS-1H, (d) BHS-2T, (e) TRP-1T, and (f) SRT7-(3 × 3)-9H pure germanane structures supported on Al_2Ge, respectively relatively stable alloy species (g) Al_4Ge_4 BHS-1T, (h) Al_3Ge_5 TRP-2T, and (i) $Al_{27}Ge_{27}$ SRT7-(3 × 3)-9T structures, respectively.

References

[1] Novoselov K S, Geim A K, Morozov S V, Jiang D, Zhang Y, Dubonos S V, Grigorieva I V and Firsov A A 2004 *Science* **306** 666

[2] Geim A K and Novoselov K S 2007 *Nat. Mater.* **6** 183

[3] Kim K S, Zhao Y, Jang H, Lee S Y, Kim J M, Kim K S, Ahn J H, Kim P, Choi J Y and Hong B H 2009 *Nature* **457** 706

[4] Novoselov K S, Geim A K, Morozov S V, Jiang D, Katsnelson M I, Grigorieva I V, Dubonos S V and Firsov A A 2005 *Nature* **438** 197

[5] Zhang Y, Tan Y W, Stormer H L and Kim P 2005 *Nature* **438** 201

[6] Wei Y P, Jia T and Chen G 2017 *Chin. Phys. B* **26** 028103

[7] Naguib M, Mochalin V N, Barsoum M W and Gogotsi Y 2014 *Adv. Mater.* **26** 992

[8] Manzeli S, Ovchinnikov D, Pasquier D, Yazyev O V and Kis A 2017 *Nat. Rev. Mater.* **2** 17033

[9] Liu J, Ma Y Q, Dai Y W, Chen Y, Li Y, Tang Y N and Dai X Q 2019 *Chin. Phys. B* **28** 107101

[10] Ren D, Tan X, Zhang T and Zhang Y 2019 *Chin. Phys. B* **28** 086104
[11] Li L, Yu Y, Ye G J, Ge Q, Ou X, Wu H, Feng D, Chen X H and Zhang Y 2014 *Nat. Nanotechnol.* **9** 372
[12] Li L, Lu S Z, Pan J, Qin Z, Wang Y Q, Wang Y, Cao G Y, Du S and Gao H J 2014 *Adv. Mater.* **26** 4820
[13] Dávila M E, Xian L, Cahangirov S, Rubio A and Le Lay G 2014 *New J. Phys.* **16** 095002
[14] Derivaz M, Dentel D, Stephan R, Hanf M C, Mehdaoui A, Sonnet P and Pirri C 2015 *Nano Lett.* **15** 2510
[15] Fukaya Y, Matsuda I, Feng B, Mochizuki I, Hyodo T and Shamoto S I 2016 *2D Mater.* **3** 035019
[16] Stephan R, Derivaz M, Hanf M C, Dentel D, Massara N, Mehdaoui A, Sonnet P and Pirri C 2017 *J. Phys. Chem. Lett.* **8** 4587
[17] Wang W and Uhrberg R I G 2017 *Beilstein J. Nanotechnol.* **8** 1946
[18] Endo S, Kubo O, Nakashima N, Iwaguma S, Yamamoto R, Kamakura Y, Tabata H and Katayama M 2018 *Appl. Phys. Express* **11** 015502
[19] Stephan R, Hanf M C, Derivaz M, Dentel D, Asensio M C, Avila J, Mehdaoui A, Sonnet P and Pirri C 2016 *J. Phys. Chem. C* **120** 1580
[20] Martinez E A, Fuhr J D, Grizzi O, Sanchez E A and Cantero E D 2019 *J. Phys. Chem. C* **123** 12910
[21] Lei B, Zhang Y Y and Du S X 2019 *Chin. Phys. B* **28** 046803
[22] He X and Li J B 2019 *Chin. Phys. B* **28** 037301
[23] Su Y and Fan X 2017 *Chin. Phys. B* **26** 108101
[24] Wang H B, Su Y and Chen G 2014 *Chin. Phys. B* **23** 018103
[25] Kresse G and Furthmüller J 1996 *Phys. Rev. B* **54** 11169
[26] Perdew J P, Burke K and Ernzerhof M 1996 *Phys. Rev. Lett.* **77** 3865
[27] Kresse G and Joubert D 1999 *Phys. Rev. B* **59** 1758
[28] Monkhorst H J and Pack J D 1976 *Phys. Rev. B* **13** 5188
[29] Kittel C 1996 *Introduction to Solid State Physics*, 7th edn. (New York: John Wiley & Sons)
[30] Garcia J C, Lima D B, Assali L V C and Justo J F 2011 *J. Phys. Chem. C* **115** 13242
[31] Li S J, Su Y and Chen G 2015 *Chem. Phys. Lett.* **638** 187
[32] Arnold C C, Xu C, Burton G R and Neumark D M 1995 *Spectroscopy* **102** 6982
[33] Lide D R 2001 *CRC Handbook of Chemistry and Physics*, 84th edn. (New York: CRC Press)
[34] Shi S, Liu Y, Zhang C, Deng B and Jiang G 2015 *Comput. Theor. Chem.* **1054** 8
[35] Fang J, Zhao P and Chen G 2018 *J. Phys. Chem. C* **122** 18669
[36] Bader R F W 1990 *Atoms in Molecules: A Quantum Theory* (Oxford: Oxford University Press)
[37] Tang W, Sanville E and Henkelman G 2009 *J. Phys.: Condens. Matter* **21** 084204
[38] Tersoff J and Hamann D R 1983 *Phys. Rev. Lett.* **50** 1998
[39] Zhang C, Chen G, Wang K, Yang H, Su T, Chan C T, Loy M M T and Xiao X 2005 *Phys. Rev. Lett.* **94** 176104
[40] Chen G, Xiao X, Kawazoe Y, Gong X G and Chan C T 2009 *Phys. Rev. B* **79** 115301
[41] Muller E, Sutter E, Zahl P, Ciobanu C V and Sutter P 2007 *Appl. Phys. Lett.* **90** 151917
[42] Zheng M M, Li S J, Su Y, Chen G and Kawazoe Y 2013 *J. Phys. Chem. C* **117** 25077
[43] Zheng M M, Ren T Q, Chen G and Kawazoe Y 2014 *J. Phys. Chem. C* **118** 7442
[44] Oughaddou H, Aufray B and Gay J M 1999 *Surf. Review. Lett.* **6** 929
[45] Oughaddou H, Sawaya S, Goniakowski J, Aufray B, Le Lay G, Gay J, Tréglia G, Bibérian J P, Barrett N, Guillot C, Mayne A and Dujardin G 2000 *Phys. Rev. B* **62** 16653
[46] Liu Y, Zhuang J, Liu C, Wang J, Xu X, Li Z, Zhong J and Du Y 2017 *J. Phys. Chem. C* **121** 16754
[47] Togo A, Oba F and Tanaka I 2008 *Phys. Rev. B* **78** 134106